Charge Exchange and Production of η Mesons and Multiple Neutral Pions in $\pi^- p$ Reactions between 654 and 1247 MeV/c†*

F. BULOS,‡ R. E. LANOU, A. E. PIFER,§ AND A. M. SHAPIRO
Brown University, Providence, Rhode Island 02912

AND

C. A. BORDNER,‖ A. E. BRENNER, M. E. LAW, E. E. RONAT,** F. D. RUDNICK,††
K. STRAUCH, AND J. J. SZYMANSKI‡‡
Harvard University, Cambridge, Massachusetts 02138

AND

P. BASTIEN, B. B. BRABSON,§§ Y. EISENBERG,** B. T. FELD, V. K. KISTIAKOWSKY,
I. A. PLESS, L. ROSENSON, AND R. K. YAMAMOTO
Laboratory for Nuclear Science, Massachusetts Institute of Technology, Cambridge, Massachusetts 02139

AND

G. CALVELLI, F. GASPARINI, L. GUERRIERO,‖‖ G. A. SALANDIN, A. TOMASIN, ‖‖
L. VENTURA, C. VOCI, AND F. WALDNER
Istituto di Fisica dell 'Universita di Padova and Istituto Nazionale di Fisica Nucleare, Sezione di Padova, Padova, Italy

(Received 2 June 1969)

An experiment designed to study the $\pi^- p$ total neutral cross section and its breakdown into several channels has been performed at eleven incident pion momenta ranging from 654 to 1247 MeV/c. Angular distributions for the charge exchange π^0 and for η^0 production are given in terms of Legendre-polynomial expansion coefficients. Forward and backward differential cross sections are presented for the charge-exchange channel and comparisons with recent dispersion-relation predictions for the forward cross section are made.

I. INTRODUCTION

IN this paper, we report the results of an experiment designed to measure detailed features of several neutral final states originating from $\pi^- p$ interactions at eleven incident pion momenta ranging from 654 to 1247 MeV/c. The experiment was performed at the Brookhaven National Laboratory Cosmotron. Preliminary results of this experiment based upon limited statistics have previously been reported.[1]

The reactions of particular interest are

$$\pi^- + p \rightarrow n + \pi^0, \tag{1}$$

$$\pi^- + p \rightarrow n + \eta^0, \tag{2}$$

$$\pi^- + p \rightarrow n + k\pi^0, \quad k = 2,3,\cdots. \tag{3}$$

The $\pi^- p$ total neutral cross section and its breakdown into the above-described channels has been measured; for processes (1) and (2), the differential cross sections have been studied in detail. Other possible reactions with neutral final states (e.g., $\pi^- + p \rightarrow \Lambda^0 + K^0$ and $\pi^- + p \rightarrow n + \omega$) have been considered only for background subtraction purposes.

The momentum interval spans the two well-known baryon resonances $N^*(1518)$ and $N^*(1688)$. In addition, the lowest momentum is below the η-meson threshold and consequently its excitation function is thoroughly covered.

Since π^0 and η^0 both have decay modes with only γ rays in the final state, a suitable detection system must have a high probability for γ-ray detection. Moreover, it must also restrict the event selection to completely neutral final states without introducing any biases into the desired measurements. These requirements resulted in the choice of a spark-chamber system containing high-Z material for γ-ray conversion and a triggering logic which selected reactions with an incident π meson entering a hydrogen target, located in the center of the spark-chamber array, and no charged particles emerging.

† Work supported in part through funds provided by the U. S. Atomic Energy Commission, under Contract Nos. At (30-1)-2098, At (30-1)-2752, and At (30-1)-2262, and in part by the Istituto Nationale di Fisica Nucleare, Italy.

* Research performed partially at Brookhaven National Laboratory, Upton, N. Y.

‡ Present address: Stanford Linear Accelerator, Palo Alto, Calif.

§ Present address: University of Arizona, Tucson, Ariz.

‖ Present address: Colorado College, Colorado Springs, Colo.

** Present address: Weizmann Institute, Rehovoth, Israel.

†† Present address: University of California, Los Angeles, Calif.

‡‡ Present address: Massachusetts State College, Salem, Mass.

§§ Present address: University of Indiana, Bloomington, Ind.

‖‖ Present address: Istituto di Fisica dell'Universita di Bari, Bari, Italy.

[1] F. Bulos, R. E. Lanou, A. E. Pifer, A. M. Shapiro, M. Widgoff, R. Panvini, A. E. Brenner, C. A. Bordner, M. E. Law, E. E. Ronat, K. Strauch, J. J. Szymanski, P. Bastien, B. B. Brabson, Y. Eisenberg, B. T. Feld, V. K. Fischer, I. A. Pless, L. Rosenson, R. K. Yamamoto, C. Calvelli, L. Guerriero, G. A. Salandin, A. Tomasin, L. Ventura, C. Voci, and F. Waldner, Phys. Rev. Letters **13**, 486 (1964); **13**, 558 (1964); in *Proceedings of the Twelfth International Conference on High-Energy Physics, Dubna, 1964* (Atomizdat, Moscow, 1966), p. 38; L. Guerriero, Proc. Roy. Soc. (London) **289**, 471 (1966).

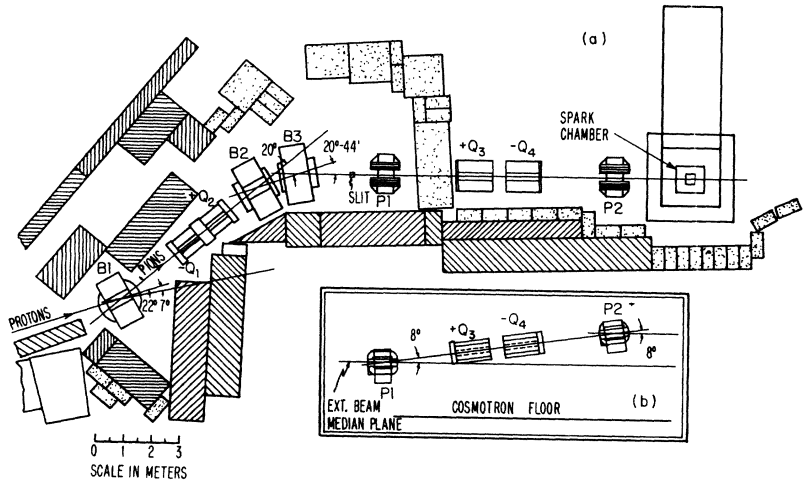

FIG. 1. Beam-transport and detector layout. See text for details.

II. EXPERIMENTAL APPARATUS

A. Beam Transport

The beam used in this experiment was designed by conventional methods, utilizing computer-calculated ray tracing and parameter optimization, to provide 3×10^3 π^-/pulse in a region 4 cm in diameter, with a relatively high momentum resolution ($\pm0.5\%$) over a wide momentum range.

In function, the beam was composed of two sections, as shown in Fig. 1. The first section, magnets B1, Q1, Q2, B2, and B3, provided momentum selection. The source of π^- for this system was a carbon target $1\times\frac{1}{2}\times14$ in. irradiated by protons (incident on its $1\times\frac{1}{2}$-in. face) from external beam 2. This target was placed about 3 in. upstream from the pole face of bending magnet B1, an 18×36-in. magnet with a 4-in. gap, which served principally to deflect pions out of the target cave and played essentially no part in momentum selection. Magnets Q1 and Q2, an 8×16-in. quadrupole pair, had a horizontal focus at the slit position. Magnets B2 and B3, both 18×36-in. bending magnets with 6-in. gaps, performed the momentum dispersion. The slit, which had Heavimet jaws, was $\frac{3}{4}$-in. horizontally by 3 in. vertically.

The function of the second group of magnets, P1, Q3, Q4, and P2, was to change the horizontal level of the beam so that it passed through the chambers and hydrogen target at the correct height of 98-in. above the floor. This placement of the high-Z chambers had the additional essential feature of removing them from the direct line of flight for any γ ray originating in the slit. Magnets P1 and P2 were pitching magnets (12×24 in. with 6-in. gap); magnets Q3 and Q4 were a quadrupole pair (8×48 in.), which provided a vertical and horizontal focus within the hydrogen target.

The magnetic fields of the momentum-resolving magnets were measured with a NMR probe and continuously monitored by previously calibrated Hall-effect probes. A precise determination of the beam momenta is provided by a method based on the kinematics of reactions (1) and (2), and is described in Appendix A.

B. Target and Detector System

The hydrogen target was molded from a 50-μ Mylar sheet into an approximately oblate spheroid form, 4 cm long and 5 cm in diameter, and placed in a stainless-steel vacuum jacket (0.25 mm thick) equipped with 50-μ-thick Mylar windows along the beam direction.

A system of four large steel-plate spark chambers[2] covered a $\frac{2}{3}(4\pi)$-sr solid angle around the target. Details of the detector system are shown schematically in Fig. 2. Each chamber was made of 50 plates, each 2 mm thick, with a total equivalent thickness of about 5.5 radiation lengths. The plates of spark chamber SP1 were provided with a beam hole, 9 cm in diameter, covered by 50-μ brass foils in order to minimize the absorption of the beam in the chamber while preserving the visibility of the incoming track. Also included were three thin-foil spark chambers whose function will be described in Sec. IV.

In order to select only reactions with neutral final states, the hydrogen target was closely surrounded by an anticoincidence shield consisting of counters C4, C5, C6, and C7. The beam was defined by the counter telescope C1, C2, C3, and by a round hole, 2.5 cm in diameter, in the anticoincidence shield (C4); the signature of a beam particle was therefore C1, C2, C3, $\bar{C}4$. Neutral events were selected by the coincidence C1, C2, C3, $\bar{C}4$, $\bar{C}5$, $\bar{C}6$, $\bar{C}7$ corresponding to the disappearance of a π^- within the anticoincidence shield.

All interactions in C3 yielding neutral final states were not distinguishable from interactions of the same kind taking place in the target solely by means of the

[2] C. Calvelli, P. Kusstatscher, L. Guerriero, C. Voci, F. Waldner, I. A. Pless, L. Rosenson, G. A. Salandin, F. Bulos, R. E. Lanou, and A. M. Shapiro, Rev. Sci. Instr. **35**, 1642 (1964); L. Guerriero, J. T. Massimo, G. A. Salandin, C. Voci, R. E. Lanou, A. E. Pifer, B. B. Brabson, and L. Rosenson, *ibid.* **37**, 118 (1966).

electronic logic. To minimize the number of these spurious events, a thickness of 1 mm was chosen for C3. Moreover, this counter was located inside the antishield to avoid an enhancement of background due to particles outside the limits of the anticoincidence hole. Such a geometry also improves the rejection efficiency of the antishield for wide-angle charged-prong interactions in C3. The comparatively low efficiency (90%) of a counter as thin as 1 mm does not affect the cross-section measurements, since it reduces the beam and the triggering counting rates by the same fraction.

Two stereo views of each of the four main chambers and of the three thin-foil chambers were photographed on a single 70-mm frame by means of the mirror system described in Ref. 2. The film used was TRI-X and the lens, which had a focal length of 190 mm, was set at $f/11$.

C. Film Scanning and Measuring

The film was scanned and measured on projectors equipped with image plane x-y digitizers having a resolution of at least 1 part in 4000. The positions of sparks in space were obtained with an average precision of ± 2 mm using standard techniques of approximately orthogonal stereo reconstruction. The main contribution to the uncertainty in the directions of γ rays arises from the finite dimension of the target. In order to minimize this error, the interaction-point coordinates transverse to the beam-particle direction were determined by measuring two or three points along the beam-particle track. The uncertainty on the longitudinal coordinate (± 2 cm maximum, from the median plane) introduces an average error of 2° in the direction of a γ ray in the most unfavorable situation, corresponding to a γ ray emitted at 90° to the beam direction. This error, as well as the resolution spread arising from the precision of the film measurements, was taken into account in the Monte-Carlo calculations performed during the subsequent analysis of the data.

III. TOTAL NEUTRAL CROSS SECTION

Full-target and empty-target data were taken at each momentum. In order to calculate the separate cross sections for each of the neutral final states detected in this experiment, we must set an absolute scale for our observed events. We do this by first calculating a total neutral cross section which is closely related to the electronic counting rates measured at the time of the exposure.

Let R be the electronic counting rate per incident pion corrected for empty-target events and for electron and muon contamination in the pion beam. This quantity can be related to the total neutral cross section by the formula

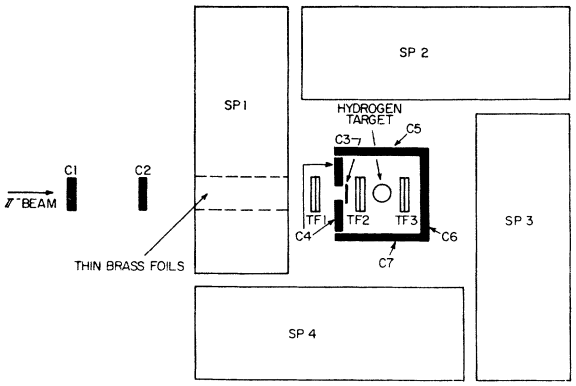

FIG. 2. Counter trigger and spark-chamber detector system. A description of this system is given in the text.

$$R=\frac{T-O}{1-\mu-\epsilon}=(1-e^{-nt\sigma_T})\times\left[\frac{\sigma_N}{\sigma_T}(1-F_1)+\left(1-\frac{\sigma_N}{\sigma_T}\right)F_2\right], \quad (4)$$

where T is the full-target counting rate

$$[=(\mathrm{C1C2C3}\bar{\mathrm{C}}4\bar{\mathrm{C}}5\bar{\mathrm{C}}6\bar{\mathrm{C}}7/\mathrm{C1C2C3C4})_{\mathrm{full}}],$$

O is the empty-target counting rate

$$[=(\mathrm{C1C2C3}\bar{\mathrm{C}}4\bar{\mathrm{C}}5\bar{\mathrm{C}}6\bar{\mathrm{C}}7/\mathrm{C1C2C3C4})_{\mathrm{empty}}],$$

ϵ is the fractional electron contamination in the beam, μ is the fractional muon contamination in the beam, n is the number of protons per $\mathrm{cm}^3=4.28\times10^{22}$, t is the average target length at liquid-hydrogen temperature ($=3.96$ cm), σ_N is the $\pi^- p$ total neutral cross section, σ_T is the $\pi^- p$ total cross section, F_1 is the fraction of neutral events that appear as charged, and F_2 is the fraction of charged events that appear as neutral. The calculation of F_1 and F_2 is described in Appendix B. Since $nt\sigma_T\ll1$ and $F_2\cong0$, expression (4) can be solved for σ_N:

$$\sigma_N\cong R/nt(1-F_1). \quad (5)$$

The σ_N which results is the measured total neutral cross section. The sum of the partial cross sections for the major reaction channels indicated by (1)–(3) plus the small background of Λ^0-K^0 and ω^0 differs from σ_N because of Dalitz-pair effects. That is, those events having internally converted γ rays can anti themselves out. The correction for this effect is dependent on the number of γ rays and consequently upon the final decomposition into the appropriate channels. We have chosen to make this correction channel by channel at the time we calculate the partial cross sections from the measured total neutral cross section. All partial cross sections quoted in this paper have had this correction made.

TABLE I. Electronic rates and correction factors. In the different columns all figures concerning formula (5) are entered. The resulting cross sections are uncorrected for Dalitz pairs.

Momentum (MeV/c)	KE (MeV)	$T\times10^3$	$O\times10^3$	$(T-O)\times10^3$	$1-\mu-\epsilon$	$1-F_1$	σ_N (mb)
654	529	1.6384	0.5422	1.0962	0.65	0.93	10.78±0.53
694	568	1.7465	0.5696	1.1769	0.69	0.93	11.03±0.53
729	603	1.8439	0.5495	1.2944	0.70	0.93	11.91±0.41
755	628	1.7846	0.5446	1.2400	0.71	0.92	11.34±0.35
811	683	1.4948	0.5069	0.9879	0.74	0.93	8.69±0.23
862	734	1.6060	0.5349	1.0711	0.76	0.93	9.15±0.41
928	799	1.8818	0.5678	1.3140	0.78	0.93	10.89±0.35
978	848	2.0602	0.5429	1.5173	0.78	0.93	12.40±0.35
1024	894	1.8780	0.5424	1.3356	0.80	0.93	10.88±0.35
1099	968	1.3291	0.4638	0.8653	0.82	0.92	6.92±0.12
1247	1115	1.0385	0.4083	0.6302	0.84	0.94	4.93±0.12

The electron contamination was measured by the showers developed in the high-Z chambers when the beam particles were allowed to trigger the system. The muon contamination was calculated[3] by computer using a Monte-Carlo method.

All quantities entering into the calculation of the total neutral cross section along with errors on the cross section are presented in Table I; the values as a function of incident momenta are shown in Fig. 3. The errors are primarily due to systematics; the major component is the uncertainty in the electron and muon contamination.

IV. MULTIPLE-π^0 SAMPLE

As seen in the previous section, the total neutral cross section has been evaluated mainly from electronic counting rates. Any further analysis has to be based on the information contained in the spark-chamber photographs.

The electronic counting rates in Table I show the contribution of nonhydrogen background interactions. We succeeded in considerably improving the signal-to-noise ratio (from 4:1 to 16:1) by inserting the two thin-foil spark chambers TF2 and TF3 just before and after the target. This addition, while not affecting appreciably the spurious triggering rate, enabled us to reject by visual inspection most of the background on an individual rather than on a statistical basis.

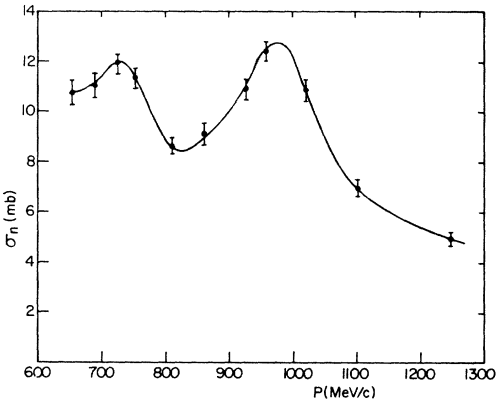

FIG. 3. Total neutral cross section for π^-p interactions. The curve is drawn to serve as a guide to the eye.

[3] A. E. Pifer, Brown University Internal Report (unpublished).

The pictures have been divided into two categories: good triggers and bad triggers. A good-trigger signature is provided by a track which shows aligned sparks in chambers SP1, TF1, and TF2 and no spark in TF3. Any different configuration in the thin-foil chambers has been called a bad trigger. All events with a good-trigger signature and at least two visible γ-ray showers have been measured.

From the reactions listed in the Introduction, it is clear that an even number of γ rays is consistently assumed to be produced in any event of our sample. Only at the two highest momenta can a three-γ-ray final state be expected from the $\pi^0\gamma$ decay of the ω^0. However, any multiplicity ranging from zero to six γ rays may be observed since some γ rays can escape detection because of our geometry and the finite thickness of the radiator plates. The breakdown of the data according to the different γ-ray multiplicities is given in Table II.

Defining as p_{jk} the probability that in our apparatus a k γ-ray parent event be seen as a j γ-ray event, the following equations hold:

$$n_j=\sum_k p_{jk}N_k, \quad k=2,3,4,6, \quad j=0,1,2,\cdots,6, \quad j\leq k \quad (6)$$

where n_j is the number of observed events with j γ rays and N_k the number of parent events with k γ rays.

The observed two-γ-ray sample, which contains information on the charge-exchange and η-meson production reactions, also has contributions from the multiple-π^0 parent events. To correct for this background, as well as to assign the correct cross section to each of the multiple-π^0 channels, least-squares fits to the parent numbers N_k have been performed at each momentum. To accomplish this, the observed sample of events with $0\leq j\leq 6$ and the relevant equations from (6) were used.

The p_{jk}'s for the geometry of our spark-chamber system were calculated using the Monte-Carlo event-

TABLE II. Scanning results for full-target data. Ambiguous events have a distribution of multiplicities essentially the same as the unambiguous. They have been excluded from all considerations except that of partial cross sections. The number of two-γ-ray events is divided in two parts to show the relative populations of the π^0 and η^0 regions, respectively.

Momentum (MeV/c)	Total triggers	Number of good triggers by γ-ray multiplicities 0–1	2 (<90°)	2 (>90°)	3	4	5	6	Ambig.
654	11 341	2930	3037	225	320	85	5	0	297
694	17 889	4122	4638	543	640	229	47	6	207
729	18 646	4903	4505	856	849	400	86	8	293
755	21 643	5211	4311	1065	1124	456	107	22	544
811	5 674	1420	1128	338	326	149	28	4	226
862	25 841	6447	4325	1316	1531	682	119	14	736
928	23 027	6024	4629	926	1411	595	92	23	550
978	20 874	5084	4257	893	1404	536	102	15	787
1024	22 878	5144	4579	904	1374	568	127	21	413
1099	22 012	5276	3732	1152	1519	674	148	26	897
1247	23 462	4917	4098	1419	1750	921	277	78	776

generator program NVERTX[4] and also an independent simulation program.[5] Phase-space-distributed events were generated simulating the $2\pi^0$ and $3\pi^0$ parent events, and then every decay γ ray was traced through the geometry of the triggering and spark-chamber systems and tagged as to whether it would develop a detectable shower and did not have the accompanying neutron interact in such a way as to trigger the anticoincidence system. The correction for neutron and γ-ray detection in the antishield, which causes the loss of a good event, is small but not negligible, and is discussed in Appendix B.

A study has been made of the dependence of the p_{jk}'s, and the cross sections which result from their use, on the production mechanism. We have used, in addition to phase space, two-π^0 production through the reaction

$$\pi^- p \rightarrow N^*(1238)+\pi^0$$
$$\searrow$$
$$n+\pi^0,$$

in which the $N^*(1238)$ is given various production and decay angular distributions. The cross sections do not depend strongly upon the model. In general, they vary by a few hundredths of a millibarn over all models tested. This variation is of the same order as, or less than, the statistical error. Consequently, we used the phase-space values for the p_{jk}'s with $k \geq 3$. The procedure had to be changed for the p_{jk}'s with $k=2$. Here, the angular distributions needed for simulating the π^0 and η^0 simulated events were those which are the final results of the experiment and therefore initially unknown. The experimentally observed bisector distributions (see Sec. V) were used first, and then the whole process of data reduction described here and in the following sections was iterated. Typically, one iteration served to produce stable values of the p_{jk}'s involved.

In addition, the p_{jk}'s are sensitive to the effective threshold energy for γ-ray detection assumed in the simulation programs. This threshold arises principally from finite plate thickness and gap inefficiency. Its best estimate, ascertained by a method described in Appendix C, is 40 ± 10 MeV. The possible systematic variation in the cross section due to this effect is again of the same order as the statistical error.

The p_{jk}'s used in the least-squares fits for the parent numbers of π^0, η^0, $2\pi^0$, and $3\pi^0$ events are given in Table III, and the results of the calculation are listed in Table IV. Table IV also gives the best value for the parent number of π^0 and η^0 events obtained by an alternative method based on angular-distribution analysis and discussed in Sec. V; it can be seen that the agreement is satisfactory.

The background contributions to the two-γ-ray sample are obtained from the values N_4, N_6, N_3, and the appropriate p_{jk}'s inserted into Eq. (6) with $j=2$.

The partial cross sections are calculated from the fitted numbers of parent events and are tabulated in Table V and plotted as a function of incident π^- laboratory momentum in Fig. 4. The corrections for Dalitz pairs, mentioned earlier, are made at this point. The resulting total neutral cross section, i.e., the sum of all known channels, is thus slightly larger than the measured σ_N. It should be noted that this fitting technique gives rise to correlated partial cross sections. The quoted errors are from the diagonal elements of the error matrix.

At the two highest momenta, contributions from $\omega^0 \rightarrow \pi^0\gamma$ and $4\pi^0$ channels are possible. It is found that neither of these channels is needed for an adequate fit at 1099 MeV/c and that only a small amount from the ω^0 channel is needed at 1247 MeV/c. The cross-section values which result for ω^0 production, assuming a branching ratio of 9.7% for the $\pi^0\gamma$ mode,[6] are consistent with bubble-chamber results[7] at the same momenta.

A very small correction must be made at the four highest momenta to account for events which arise

[4] A. E. Brenner, C. A. Bordner, and E. E. Ronat, Rev. Sci. Instr. **37**, 36 (1966).

[5] A. Tomasin, thesis, University of Padova, 1965 (unpublished).

[6] Average value compiled by A. Rosenfeld, N. Barash-Schmidt, A. Barbaro-Galtieri, L. Price, P. Söding, C. Wohl, and M. Roos, Rev. Mod. Phys. **40**, 77 (1968).

[7] R. Kraemer, L. Madansky, M. Meer, M. Nussbaum, A. Pevsner, C. Richardson, R. Strand, R. Zdanis, T. Fields, S. Orenstein, and T. Toohig, Phys. Rev. **136**, B496 (1964).

TABLE III. The P_{jk} probabilities. The second subscript denotes the parent configuration and the first indicates the observed γ-ray multiplicity. (A) contains those for possible 2γ parents, (B) for 4γ parents, (C) for 6γ parents, and (D) for 3γ ($\omega^0 \to \pi^0\gamma$) parents. The statistical errors on these P_{jk}'s are those appropriate to a sample of 20 000 events thrown for π^0 and η^0, 10 000 events for $2\pi^0$, 5000 events for $3\pi^0$, and 10 000 for ω^0. The subscripts $0+1$ indicate the sum of $P_{0,k}+P_{1,k}$ and the subscripts 2^- and 2^+ indicate the $P_{2,k}$ for opening angles less than and greater than 90°, respectively.

(A) π^0 and η^0 parents (2γ)

Momentum (MeV/c)	P_{0+1,π^0}	P_{2-,π^0}	P_{0+1,η^0}	P_{2+,η^0}
654	0.453	0.487	...	...
694	0.428	0.523	0.555	0.382
729	0.451	0.490	0.545	0.392
755	0.471	0.470	0.544	0.391
811	0.495	0.447	0.549	0.388
862	0.549	0.397	0.544	0.393
928	0.515	0.429	0.551	0.388
978	0.493	0.452	0.526	0.410
1024	0.494	0.451	0.567	0.373
1099	0.518	0.425	0.512	0.420
1247	0.475	0.467	0.501	0.434

(B) $2\pi^0$ parents (4γ)

Momentum (MeV/c)	$P_{0+1,2\pi^0}$	$P_{2-,2\pi^0}$	$P_{2+,2\pi^0}$	$P_{3,2\pi^0}$	$P_{4,2\pi^0}$
654	0.277	0.187	0.184	0.214	0.040
694	0.205	0.176	0.180	0.272	0.089
729	0.242	0.181	0.179	0.244	0.055
755	0.238	0.181	0.177	0.248	0.058
811	0.177	0.171	0.169	0.286	0.088
862	0.206	0.177	0.168	0.275	0.075
928	0.185	0.174	0.161	0.292	0.089
978	0.182	0.173	0.157	0.296	0.093
1024	0.166	0.170	0.153	0.308	0.104
1099	0.201	0.180	0.147	0.288	0.087
1247	0.170	0.173	0.133	0.312	0.125

(C) $3\pi^0$ parents (6γ)

Momentum (MeV/c)	$P_{0+1,3\pi}$	$P_{2-,3\pi}$	$P_{2+,3\pi}$	$P_{3,3\pi}$	$P_{4,3\pi}$	$P_{5,3\pi}$	$P_{6,3\pi}$
654	0.110	0.121	0.123	0.295	0.162	0.053	0.004
694	0.056	0.073	0.085	0.279	0.237	0.137	0.029
729	0.079	0.100	0.106	0.293	0.204	0.085	0.101
755	0.076	0.099	0.104	0.292	0.209	0.077	0.011
811	0.037	0.031	0.072	0.271	0.251	0.164	0.025
862	0.053	0.079	0.087	0.284	0.249	0.101	0.026
928	0.041	0.068	0.076	0.276	0.261	0.123	0.022
978	0.039	0.068	0.074	0.273	0.264	0.125	0.023
1024	0.031	0.059	0.065	0.265	0.274	0.143	0.028
1099	0.051	0.085	0.082	0.278	0.246	0.102	0.027
1247	0.038	0.064	0.059	0.251	0.269	0.145	0.029

(D) ω^0 parents (3γ)

Momentum (MeV/c)	$P_{0+1,\omega}$	$P_{2(<90°),\omega}$	$P_{2(>90°),\omega}$	$P_{3,\omega}$
1099	0.253	0.125	0.287	0.263
1247	0.233	0.123	0.280	0.283

from the production of Λ^0 and K^0 and in which the decay products are all neutral or escape detection. This correction is made by using published[8,9] cross sections and branching ratios to predict the number of events to be subtracted from each γ-ray topology before the fit for parents. This correction causes its largest effect in the η^0 cross section; typically it amounts to 5% for η^0 and 0.3% for π^0.

V. π^0 AND η^0 SAMPLES

A. Separation of π^0 and η^0 Events

In order to separate the contributions to the two-γ-ray sample from charge-exchange and η^0 production reactions, an analysis has been performed based on the kinematical properties of particles decaying into two γ rays. It is in fact possible to transform γ-ray directions from the laboratory system to the center-of-mass system without knowing the γ-ray energies. In the center-of-mass system the two γ rays, coming from the decay of a monoenergetic particle, show the characteristic opening-angle distribution[10]

$$\frac{dn}{d\Theta}=\frac{(m_0/p)\cos\tfrac{1}{2}\Theta}{2\sin^2(\tfrac{1}{2}\Theta)[(E/m_0)^2\sin^2(\tfrac{1}{2}\Theta)-1]^{1/2}}, \quad (7)$$

the decay of the parent particles being isotropic in their own rest frame. E and p are the center-of-mass energy and momentum of the decaying particle of mass m_0. It is apparent that most of the events are expected in a narrow angular region close to the minimum opening angle defined by

$$\sin\tfrac{1}{2}\Theta_{\min}=m_0/E. \quad (8)$$

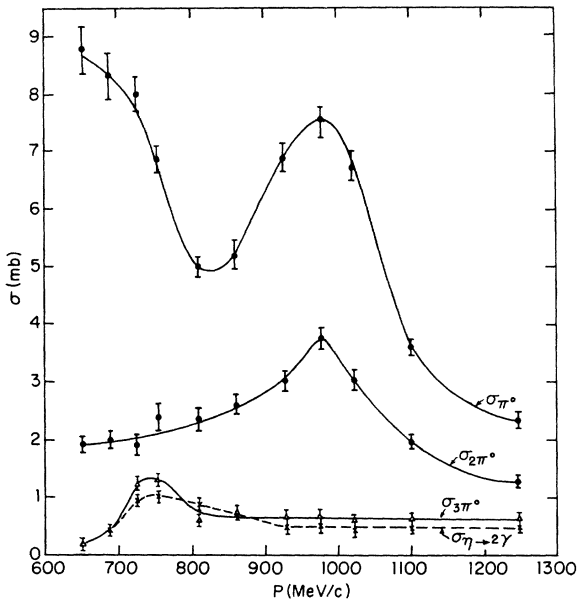

FIG. 4. Partial cross sections for charge exchange (π^0), $2\pi^0$, $3\pi^0$, and η^0 production. The curves are drawn to serve as guides to the eye.

[8] J. Steinberger, in *1958 Annual Conference on High-Energy Physics at CERN*, edited by B. Ferrett (CERN Scientific Information Service, Geneva, 1958), p. 148.

[9] F. S. Crawdord, in *Proceedings of the International Conference on High-Energy Physics, CERN, 1962*, edited by J. Prentki (CERN Europan Organization for Nuclear Research, Geneva, 1962), p. 270.

[10] See, e.g., G. Källén, *Elementary Particle Physics* (Addison-Wesley Publishing Co., Reading, Mass., 1964), p. 32.

TABLE IV. Numbers of parent events. (1) and (2) refer to the methods described in Secs. IV and V, respectively; in particular, the χ^2 probability refers to the fit described in Sec. III.

Momentum (MeV/c)	$\pi^0(1)$	$\pi^0(2)$	$\eta^0(1)$	$\eta^0(2)$	$2\pi^0$	$3\pi^0$	ω^0	$P(\chi^2)$
654	5706± 75	5600±139	...	...	1231± 72	142± 37	...	0.14
694	8211± 94	8299±172	439± 69	455± 41	1942±109	392± 48	...	0.70
729	8297±106	8080±176	981± 89	964± 68	1980±183	1270±100	...	0.07
755	7951±111	7973±179	1168± 98	1193± 85	2744±204	1452±111	...	0.15
811	2086± 52	2223± 95	364± 45	494± 53	961± 72	246± 36	...	0.15
862	8752±119	8780±209	1220±104	1226± 99	4362±182	1247± 93	...	0.13
928	9305±114	9528±217	650± 90	784± 84	3994±149	831± 71	...	0.04
978	7957±105	8334±191	555± 82	499± 84	3914±146	743± 69	...	0.11
1024	8393±108	8849±200	549± 85	707± 88	3767±135	771± 67	...	0.02
1099	6972±107	6851±168	1042± 87	1117± 99	3818±179	1392±102	...	0.60
1247	6927±106	7003±165	1533± 84	1563±105	3701±166	1928±105	100±50	0.16

A typical center-of-mass opening-angle distribution is shown in Fig. 5(a). The positions of the two peaks correspond to the $\Theta_{\min}$'s for π^0 and η^0. An unambiguous separation of the events into the two categories is clearly possible and this is true of all momenta covered by our experiment. It is evident as well that there is a background because there are events at opening angles smaller than $\Theta_{\min}(\pi^0)$ and there is an excess of events in the region between $\Theta_{\min}(\pi^0)$ and $\Theta_{\min}(\eta^0)$. In Fig. 5(b) the opening-angle distribution of background events is shown; it is normalized to the contamination calculated from the $2\pi^0$ and $3\pi^0$ parent events and the p_{jk}'s. Its shape is derived from the distribution of the opening angle between all pairs of γ rays observed in the three-γ-ray sample. Monte Carlo simulation indicates that the opening-angle distributions originating from events of higher multiplicity and detected as either two- or three-γ-ray events are approximately the same, independent of the model. The subtracted two-γ-ray opening-angle distribution is shown in Fig. 5(c). Superimposed on this histogram is a Monte-Carlo-calculated curve (see Sec. V B) which takes into account all the experimental factors for the π^0 and the η^0. The curves are separately normalized to the π^0 and η^0 regions of the histogram. χ^2 tests between the histograms and the Monte Carlo curves have been made. At all energies the χ^2 probabilities were acceptable in both the π and η regions for the incident-pion energy and choice of the low-energy γ-ray-detector cutoff. It is evident that the shapes of the experimental samples after $2\pi^0$ and $3\pi^0$ subtractions are the same as the shapes predicted by the Monte Carlo calculation. This indicates that the subtractions are correctly normalized and that the various experimental factors are correctly understood, independent of the numbers of π^0 and η^0 parents.

Unlike the peaked opening-angle distributions characteristic of π^0 and η^0, the multiple-pion events observed as two-γ-ray events exhibit a distribution in Θ which spans 0°–180°. Thus, judicious cuts in Θ allow us to obtain highly enriched, unbiased samples of π^0 and η^0 events, with essentially no mixing between them and only a small percentage of background multiple-pion events.

B. Method of Determining Angular Distributions

For both the π^0 and η^0 samples, we are interested in the center-of-mass production angular distribution of the unobserved parent particle. Since we do not measure the γ-ray energy in this experiment, there is an ambiguity between the two possible kinematical solutions for the direction of the parent particle. Our analysis procedure then is to determine the bisector direction of the two-γ-ray opening angle in the $\pi^- p$ center-of-mass system. The distribution of these bisectors can be

TABLE V. Partial cross sections. All cross sections are in mb. The errors quoted are statistical only. σ is the sum of all neutral channels, i.e., the total neutral cross section.

Momentum (MeV/c)	π^0	η^0 ($\to 2\gamma$)	$2\pi^0$	$3\pi^0$	ω ($\pi^0\gamma$)	ΛK (neutrals)	σ	$\eta^0 \to 3\pi^0/\eta^0 \to 2\gamma$
654	8.78±0.44	...	1.92±0.14	0.22±0.06	...	...	10.92	...
694	8.33±0.41	0.45±0.07	1.99±0.15	0.41±0.05	...	...	11.18	0.91±0.18
729	7.97±0.29	0.94±0.09	1.92±0.19	1.25±0.11	...	...	12.08	1.33±0.17
755	6.84±0.23	1.00±0.09	2.39±0.19	1.28±0.10	...	...	11.51	1.28±0.15
811	5.03±0.17	0.96±0.11	2.30±0.16	0.51±0.08	...	...	8.80	0.53±0.10
862	5.19±0.24	0.72±0.07	2.62±0.16	0.76±0.07	...	...	9.29	1.06±0.14
928	6.92±0.23	0.48±0.07	3.01±0.14	0.63±0.06	...	0.04	11.08	1.31±0.24
978	7.51±0.23	0.52±0.08	3.74±0.17	0.72±0.07	...	0.10	12.59	1.38±0.25
1024	6.74±0.23	0.44±0.07	3.06±0.15	0.63±0.06	...	0.18	11.05	1.43±0.26
1099	3.60±0.08	0.53±0.05	1.99±0.10	0.73±0.06	...	0.18	7.03	1.38±0.17
1247	2.36±0.07	0.52±0.03	1.28±0.07	0.67±0.04	0.11±0.05	0.06	5.00	1.29±0.11

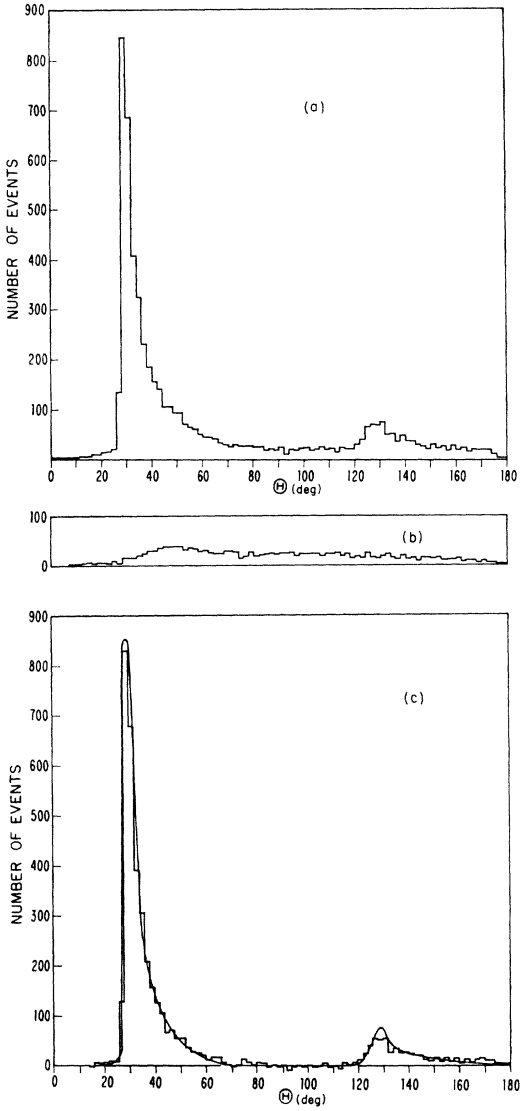

FIG. 5. Center-of-mass γ-ray opening-angle distribution for $p=862$ MeV/c. (a) Unsubtracted 2γ sample. (b) Normalized subtraction for 2γ sample. (c) Subtracted 2γ-ray opening-angle distribution. The curve is the smoothed predicted Monte Carlo result. A χ^2 test between the subtracted 2γ sample and the Monte Carlo predictions gives 90.5 for 90 degrees of freedom.

uniquely related to the parent-particle direction distribution.

As indicated earlier, there is some background contamination from multiple-pion events, which must be subtracted from the samples. A very good approximation to the distribution which must be subtracted is given by the bisector distribution of the background two-γ-ray sample, obtained as described in Sec. V A, with the appropriate cuts in Θ. In fact, the shape of this background distribution is almost independent of the cut in Θ. The appropriate normalization of the subtracted distribution comes from the evaluated number of parent $2\pi^0$ and $3\pi^0$ events and the Monte Carlo estimates of the fraction of these observed as two-γ-ray events within the appropriate region of Θ.

We have used the Monte-Carlo technique to fold additional experimental factors (e.g., measurement resolution, finite target thickness, and detection efficiency) into the transformation relating the parent-particle direction and the bisector direction distributions. Let $m(x',x)$ be the probability density that a parent particle produced in the direction defined by $x=\cos\theta$ be detected as a pair of γ rays with bisector direction defined by $x'=\cos\theta'$; then the distribution of bisectors $n'(x')$ is related to the parent-particle distribution $n(x)$ by

$$n'(x')dx'=dx'\int_{-1}^{+1} m(x',x)n(x)dx. \tag{9}$$

If we express $n(x)$ as an expansion in Legendre polynomials, $P_l(x)$, we have

$$n(x)=\sum_{l=0}^{l_{\max}} C_l P_l. \tag{10}$$

Substituting this into Eq. (9),

$$n'(x')dx'=dx'\int_{-1}^{+1}\Big(\sum_{l=0}^{l_{\max}} C_l P_l\Big)m(x',x)dx. \tag{11}$$

Experimentally, we look at a histogram of the γ-ray bisector cosines. If we replace the function $n'(x')dx'$ by n_i, where n_i is the experimental number of bisectors in the ith bin and correspondingly write $m(x',x)dx'$ as $m_i(x)$, then

$$n_i=\int_{-1}^{+1}\Big(\sum_{l=0}^{l_{\max}} C_l P_l\Big)m_i(x)dx = \sum_{l=0}^{l_{\max}} C_l\int_{-1}^{+1} P_l(x)m_i(x)dx. \tag{12}$$

These integrals can be represented as the elements of the complete transformation matrix M_{il}, which we define as

$$M_{il}=\int_{-1}^{+1} P_l(x)m_i(x)dx. \tag{13}$$

The M_{il}'s are calculated in a Monte-Carlo program which takes into account the possibility of a γ ray or neutron associated with the event triggering the anticoincidence counter, as well as cuts applied to the opening-angle distribution, effective low-energy cutoff, and experimental resolution. The actual computation of the integrals makes use of the fact that we can average over the right-hand side of Eq. (13), writing $M_{il}=2\langle P_l m_i\rangle_{\rm av}$, where

$$\langle P_l m_i\rangle_{\rm av}=\frac{1}{N}\sum_{n=1}^{N} P_l(x_n)\delta_n. \tag{14}$$

TABLE VI. Coefficients of Legendre-polynomial expansion for π^0. Cross sections are in mb and mb/sr; the errors quoted (in parentheses) in this table include only those of the fit. (Note that these errors are the diagonal errors only; the full error matrix is given in Table X.) The events used in the fit are in the range $\Theta_{\min}-5° \leq \Theta \leq \Theta_{\min}+10°$.

P (MeV/c)	k (MeV/c)	$1/k^2$ (mb)	σ (mb)	$(d\sigma/d\Omega)$ (0°)	$(d\sigma/d\Omega)$ (180°)	C_0	C_1	C_2	C_3	C_4	C_5	C_6	C_7	C_8	P (χ^2)
654	418.1	2.23	8.78	4.16	0.55	0.322	0.532	0.516	0.209	0.180	0.090	0.067	...	...	0.40
			(0.44)	(0.31)	(0.12)	(0.008)	(0.017)	(0.022)	(0.027)	(0.031)	(0.034)	(0.038)			
694	436.3	2.05	8.33	3.48	0.47	0.332	0.522	0.537	0.164	0.110	0.069	0.012	...	...	0.86
			(0.41)	(0.24)	(0.08)	(0.007)	(0.014)	(0.018)	(0.022)	(0.025)	(0.028)	(0.030)			
729	451.8	1.91	7.97	3.01	0.35	0.345	0.455	0.516	0.161	0.085	0.108	−0.030	...	...	0.01
			(0.29)	(0.19)	(0.08)	(0.008)	(0.015)	(0.019)	(0.022)	(0.026)	(0.030)	(0.032)			
755	463.0	1.82	6.84	2.24	0.15	0.312	0.319	0.417	0.145	0.026	0.136	−0.069	...	...	0.13
			(0.23)	(0.15)	(0.07)	(0.007)	(0.014)	(0.018)	(0.020)	(0.024)	(0.028)	(0.031)			
811	486.7	1.64	5.01	1.62	0.12	0.253	0.072	0.354	0.151	−0.013	0.250	−0.045	...	...	0.17
			(0.17)	(0.17)	(0.10)	(0.011)	(0.022)	(0.026)	(0.029)	(0.035)	(0.042)	(0.048)			
862	507.6	1.51	5.19	1.73	−0.03	0.296	−0.070	0.433	0.278	−0.035	0.420	−0.084	...	...	0.10
			(0.24)	(0.12)	(0.05)	(0.007)	(0.014)	(0.015)	(0.016)	(0.019)	(0.023)	(0.025)			
928	533.7	1.37	6.92	2.74	−0.07	0.415	−0.086	0.694	0.426	0.059	0.720	−0.159	...	...	0.18
			(0.23)	(0.14)	(0.06)	(0.010)	(0.020)	(0.021)	(0.023)	(0.028)	(0.032)	(0.034)			
978	552.9	1.27	7.51	3.51	0.08	0.479	0.023	0.827	0.501	0.198	0.877	−0.096	...	...	0.45
			(0.23)	(0.18)	(0.08)	(0.012)	(0.025)	(0.027)	(0.030)	(0.035)	(0.040)	(0.044)			
1024	570.5	1.20	6.74	2.82	0.25	0.454	−0.020	0.738	0.323	0.205	0.788	−0.091	...	...	0.14
			(0.23)	(0.16)	(0.08)	(0.011)	(0.022)	(0.024)	(0.023)	(0.033)	(0.037)	(0.039)			
1099	597.3	1.09	3.60	1.35	0.37	0.278	0.016	0.270	0.061	0.143	0.457	0.165	−0.062	−0.206	0.39
			(0.08)	(0.10)	(0.08)	(0.008)	(0.014)	(0.018)	(0.020)	(0.022)	(0.027)	(0.029)	(0.033)	(0.036)	
1247	648.4	0.93	2.36	0.24	0.51	0.211	0.019	0.191	−0.074	0.050	0.055	0.075	−0.156	−0.105	0.17
			(0.07)	(0.04)	(0.07)	(0.005)	(0.009)	(0.023)	(0.015)	(0.017)	(0.019)	(0.021)	(0.024)	(0.026)	

The summation extends over all of the N events simulated in the Monte-Carlo program; x_n is the cosine of the production angle of the nth event, and δ_n is 1 or zero depending upon whether the event has satisfied all requirements or not. The simulated events were picked at random out of a distribution of directions which was isotropic.

The final expression for the expected population of the bisector distribution is given by

$$n_i = \sum_{l=0}^{l_{\max}} C_l M_{il}. \tag{15}$$

The problem of determining the π^0 or η^0 angular distribution thus reduces to performing a least-squares fit of the experimental distribution of bisectors to Eq. (15) with parameters C_l of the π^0 or η^0 distribution expansion. Thus we obtain directly the Legendre-polynomial expansion coefficients for the π^0 or η^0 distributions.

C. π^0 and η^0 Angular Distributions

The least-squares fits described in the previous section were performed on each sample after the appropriate background had been subtracted. The subtraction ranged from 1 to 3% of the raw π^0 sample and up to 40% for the η^0 sample. In addition to these subtractions, at the four highest momenta a small subtraction was made for contaminants in the η^0 sample arising from the neutral decay of the Λ^0. The angular distribution for this contaminant was obtained by a Monte Carlo calculation and the normalization calculated from the known cross sections.

At each momentum for both the π^0 and the η^0 samples, a series of least-squares fits was made with values of $l_{\max}$ from 1 to 10. For the π^0 fits, where the data were adequate, each $\cos\theta'$ bin, 0.025 wide, was required to have a total fractional error, including estimated systematics in addition to the statistical error, less than 0.3. If any given bin did not meet this requirement, that bin was merged with an adjacent bisector bin. This process was continued when necessary until the test was satisfied. The same procedure was followed for the η^0 fits, except that the data were initially treated with each $\cos\theta'$ bin 0.10 wide. By this fitting procedure we obtained also the total number of parent π^0 and η^0 events in the samples; they are entered in Table IV.

The appropriate $l_{\max}$ at each momentum was chosen with the following considerations. First, in order to facilitate the use of the data in phase-shift analysis, where expansions are normally made of the amplitudes directly, we have elected to have the maximum value of l always even. In no case do the C_l's with $l<l_{\max}$ change outside the quoted errors as a result of this choice. The last coefficient is sometimes consistent with zero; however, the error on this coefficient is relevant for such analysis. The quoted errors are the diagonal elements of the error matrix; since their values are correlated, we also give the full-error matrices in Appendix D. Secondly, for a given beam momentum, that value of $l_{\max}$ was chosen where the χ^2 probability had clearly reached its asymptotic value as a function of $l_{\max}$. Furthermore, the value of $l_{\max}$ was never allowed to decrease at momenta above where it was first needed.

The Legendre-polynomial coefficients normalized according to

$$\sigma_0 = (4\pi/k^2)C_0, \tag{16}$$

where σ_0 is the π^0 or η^0 production cross section and k is

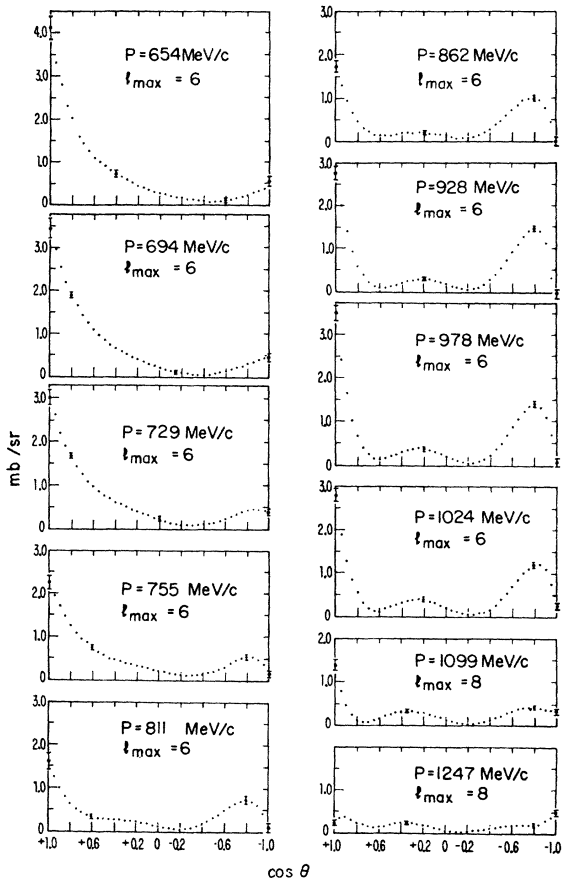

FIG. 6. Center-of-mass charge-exchange angular distributions for the π^0. Typical error bars are shown.

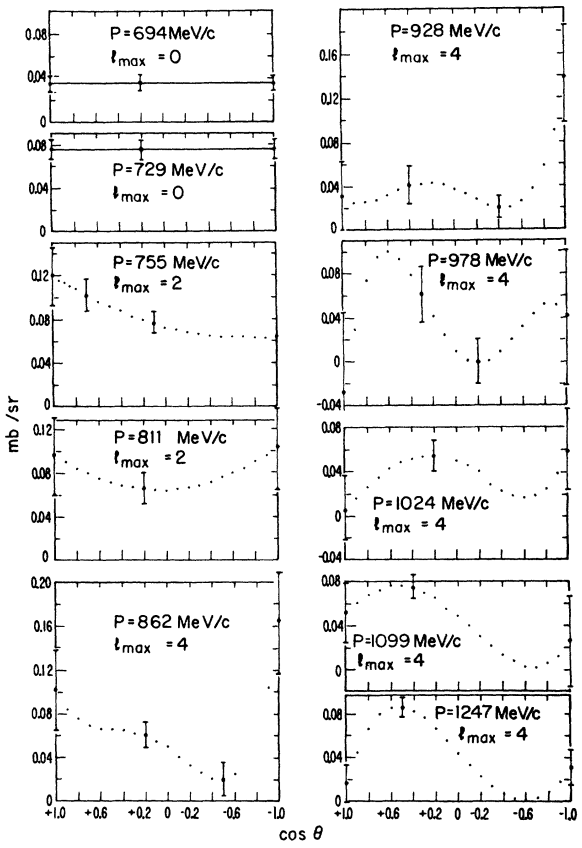

FIG. 7. Center-of-mass η^0 production angular distributions.

the π^- momentum in the center-of-mass system, are given in Tables VI and VII for π^0 and η^0, respectively. Differential cross sections can then be obtained as

$$\left(\frac{d\sigma}{d\Omega}\right)_{\text{c.m.}} = \frac{1}{k^2}\sum_{l=0}^{l_{\max}} C_l P_l(\cos\theta). \qquad (17)$$

Also given in the same tables are the forward and backward differential cross sections, calculated from Eq. (17), as well as the χ^2 probabilities of the best fits.

Plots of the π^0 and η^0 differential cross sections are given in Figs. 6 and 7, respectively; in Fig. 8 the behavior of the Legendre-polynomial expansion coefficients as a function of momentum is shown, for the π^0 case.

It should be remarked that the fits were made on a data sample with a quite narrow cut on Θ as given in Table VI. Typically, 50–70% of all events in each of the π^0 and η^0 distributions were included within these cuts. The complete analysis was also performed on a sample of data with a wider cut, which always contained more than 75% of all the events in each distribution. Within our statistics there were no differences in the results at all momenta for both samples. The narrower cut, with fewer events participating in the fits, gave results with about the same propagated errors on the coefficients of the series expansions as the wider cut. This is due to the fact that the subtracted contaminant angular distributions, with associated errors, were larger for the sample with the wider Θ cut.

Finally, Fig. 9 illustrates at 729 MeV/c a comparison of the observed bisector data (solid histogram), the fitted π^0 distribution similarly binned (dotted curve), and the Monte Carlo-predicted bisector distribution (dotted histogram) based upon the fitted distribution. The fitted distribution is normalized to the total number of π^0 parents. Thus the difference between the number of observed events in each bin and that of the predicted bisectors is the total correction, i.e., it includes bisector opening-angle cut, low-energy γ-ray cutoff, geometric detection efficiency, and opening-angle bisector to π^0 direction smearing.

VI. EMPTY-TARGET EVENTS

At each momentum a similar analysis has been undertaken on the empty-target samples. It was found that the split among the different multiplicities and the angular distributions as well agree within statistics with the corresponding full-target case. For this reason

TABLE VII. Coefficients of the Legendre-polynomial expansion for η^0. The errors quoted (in parentheses) in this table include only those of the fit. (Note that these errors are diagonal errors only; the full error matrix is given in Table XI.) The events used in the fit are in the range $\Theta_{\min}-5°\leq\Theta\leq\Theta_{\min}+10°$.

P (MeV/c)	C_0	C_1	C_2	C_3	C_4	$P(\chi^2)$	$\sigma_{\eta^0}(\rightarrow 2\gamma)$ (mb)
694	0.018	...	...	...	...	0.41	0.45
	(0.002)						(0.07)
729	0.041	...	...	...	...	0.55	0.94
	(0.003)						(0.09)
755	0.046	0.016	0.007	...	...	0.13	1.00
	(0.003)	(0.007)	(0.010)				(0.09)
811	0.048	−0.003	0.014			0.12	0.96
	(0.006)	(0.011)	(0.017)				(0.11)
862	0.041	0.008	0.030	−0.029	0.024	0.79	0.72
	(0.003)	(0.007)	(0.009)	(0.013)	(0.020)		(0.07)
928	0.028	−0.013	0.016	−0.027	0.019	0.20	0.48
	(0.003)	(0.007)	(0.009)	(0.013)	(0.020)		(0.07)
978	0.033	0.016	0.014	−0.049	−0.047	0.96	0.52
	(0.006)	(0.12)	(0.016)	(0.025)	(0.039)		(0.08)
1024	0.029	0.003	−0.013	−0.025	0.010	0.64	0.44
	(0.004)	(0.007)	(0.011)	(0.015)	(0.020)		(0.07)
1099	0.041	0.041	−0.009	−0.029	0.006	0.61	0.53
	(0.004)	(0.007)	(0.010)	(0.018)	(0.025)		(0.05)
1247	0.047	0.045	−0.011	−0.054	−0.008	0.52	0.52
	(0.003)	(0.006)	(0.008)	(0.010)	(0.015)		(0.03)

it has not been necessary to make the empty-target subtractions for the angular distributions. The cross sections have been scaled as was indicated in Sec. III.

VII. DISCUSSION OF RESULTS

A. Partial Cross Sections

The general features of the partial cross sections for reactions (1)–(3) are shown in Fig. 4. It can be seen that around 700 MeV/c the inelastic processes, especially $3\pi^0$ and η^0 production, are relatively predominant; the charge-exchange cross section indeed shows only a shoulder. Moreover, within the inelastic processes the η^0 and $3\pi^0$ productions show maxima, while the $2\pi^0$ cross section is quite constant. At 900 MeV/c the situation is just the opposite; the elastic channel and $2\pi^0$ production show marked peaks, while the η^0 and $3\pi^0$ production are both constant. Quantitatively, the charge-exchange cross section is the dominant one at all momenta; the $2\pi^0$ cross section is about one-quarter the value of charge exchange at the lower energies and one-half at the higher energies. The peak in the $2\pi^0$

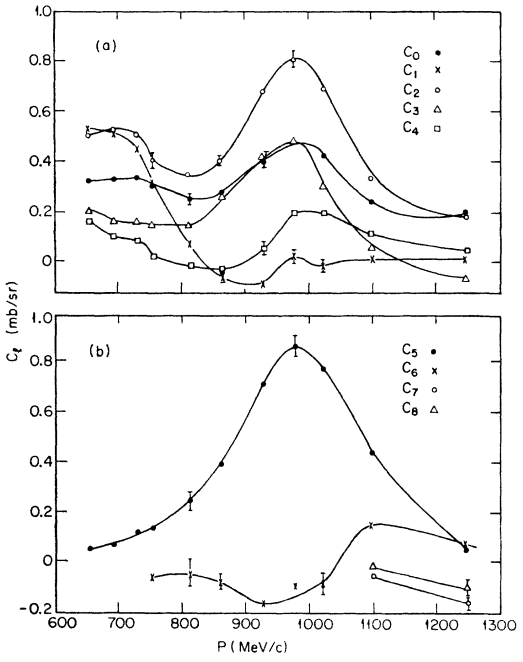

FIG. 8. Legendre-polynomial expansion coefficients for charge exchange as a function of incident π^- momentum.

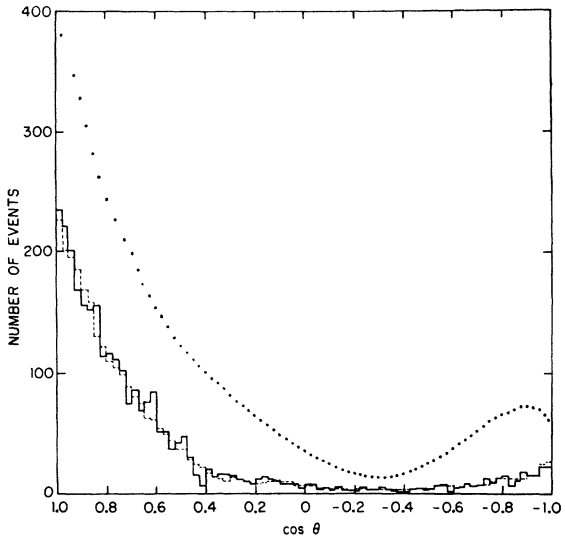

FIG. 9. An illustration at $p=729$ MeV/c of the differences between the observed bisector distribution (solid histogram), the fitted π^0 angular distribution (dotted curve) normalized to the total number of π^0 parents, and the Monte Carlo-predicted bisector distribution (dashed histogram).

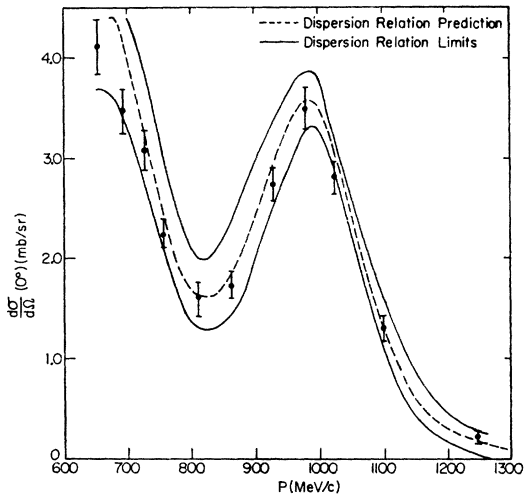

FIG. 10. Forward differential cross section $(d\sigma/d\Omega)(0°)$ for the π^0 in charge-exchange scattering. The dispersion-relation predictions from Carter (Ref. 11) are shown along with the estimated limits.

cross section may be evidence for an appreciable decay mode of $N^*(1688)$ into a final state $n\pi^0\pi^0$; on the contrary, no evidence for such a mode is indicated for $N^*(1518)$. The $\eta \to 2\gamma$ and $3\pi^0$ cross sections are nearly equal at all momenta above η^0 threshold with a magnitude about one-half that of the $2\pi^0$; they peak at about 750 MeV/c. In fact, their shapes are so similar it is suggestive that the dominant contribution to the $3\pi^0$ sample comes from the decay of the η^0 into $3\pi^0$. Consequently, it is possible to make an estimate of the upper limit of the branching ratio

$$R=(\eta \to 3\pi^0)/(\eta \to 2\gamma). \tag{18}$$

If all three π^0's are taken as coming from η^0, then $R\leq 1.19\pm 0.06$. In this case, the value of R is the average derived from all momenta above η^0 threshold and the error is the statistical error on this average. The individual ratios R at each of the momenta going into this average are listed in the last column of Table V. If, instead, one assumes that there is some non-η^0 background that should be subtracted from the $3\pi^0$ sample, then a different value of R can be obtained. In this experiment we measure a $3\pi^0$ cross section of 0.22 mb at a momentum just below η^0 threshold. Taking this value to be the non-η^0 background to be subtracted at all momenta, a value for R is found to be 0.82 ± 0.06. To give an estimate to the range of R values possible in this experiment under the assumption that there is some non-η^0 background, we may take the error on the 0.22 mb to be 100%. Thus, the previous value ($R\leq 1.19\pm 0.06$) corresponds to zero non-η^0 background and $R=0.45\pm 0.06$ corresponds to 0.44 mb of background. The currently accepted[6] value for R is 0.77 ± 0.09.

B. Total Neutral Cross Section

As seen in Fig. 3, the measured total neutral cross section shows two peaks around 600 and 900 MeV. These are centered at 729 and 978 MeV/c (i.e., $\sim$1514 and $\sim$1660 MeV for the center-of-mass energy). While the latter value is in agreement with previous measurements of the peak position in total and elastic $\pi^- p$ scattering, the former is somewhat higher.

We believe there is little meaning in directly comparing the σ_N's from different experiments, as is frequently done in the literature, since the available measurements come from different setups with different normalization and correction factors, which depend not only on the relative sizes of the partial cross sections but also upon the particular geometry involved.

C. π^0 Differential Cross Section

Since these data in their most preliminary form[1] appear in nearly all pion-nucleon phase-shift analyses to date, a direct comparison with the results of these analyses will not be made here. Rather, we will point out some of the features of the data and their form of presentation which we hope will facilitate their use in refined phase-shift analyses.

(1) The forward cross section (Fig. 10) is compared with the dispersion-relation prediction calculated from the recent reevaluation of quantities by Carter.[11] The data are in agreement with the predictions at all momenta.

(2) The backward cross section (Fig. 11) exhibits a maximum near 600 MeV and a strong minimum near 900 MeV.

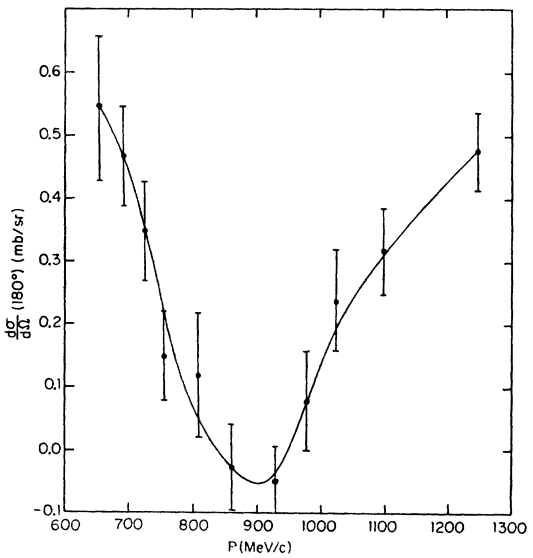

FIG. 11. Backward differential cross section $(d\sigma/d\Omega)(180°)$ for the π^0 in charge-exchange scattering.

[11] A. A. Carter, Cavendish Laboratory Report, 1968 (unpublished).

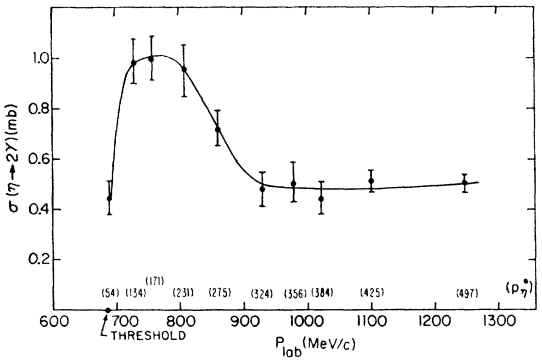

FIG. 12. The η^0 excitation curve showing the cross section for $\eta \rightarrow 2\gamma$ as a function of the incident π^- laboratory momentum p_{lab} and the η^0 center-of-mass momentum P_η^*. The solid curve serves only as a guide to the eye.

(3) The graph of the Legendre-polynomial coefficients (Fig. 8) shows the well-known freatures of the resonances in the vicinity of 600 and 900 MeV.

As was mentioned in Sec. V, we have included in this paper (Appendix D) the error matrices of the Legendre-polynomial coefficients for the fits chosen. It should be noted that these are the statistical errors only and that there are normalization errors resulting from the uncertainty in the partial cross sections for charge exchange. These additional errors have been included in the values quoted for the 0° and 180° cross sections.

D. η^0 Differential Cross Section

The η^0 differential cross sections (Fig. 7) are isotropic at the first two momenta. At higher momenta some structure gradually enters, which we were insensitive to in our preliminary low-statistics data.[1] This is consistent with the linear rise[1,12] of the excitation curve, shown in Fig. 12, and indicates S-wave production near threshold.

It has been suggested[12] that a geometry which does not cover the full 4π solid angle can lead to insensitivity in distinguishing between certain types of angular distributions. Whereas our preliminary data suffered from lack of statistics, this suggestion is not relevant to our geometry as is discussed in Appendix E. With the final sample, presented here, nonisotropy is readily distinguished at all momenta and the errors quoted on the coefficients accurately reflect the probability that the inferred coefficients might be different from the true ones. In general character, the η^0 differential cross-section curves presented here are in general agreement with those in Ref. 12. It should be noted that although they are consistent at each energy within the quoted errors, the partial η cross sections appear to be systematically of the order of 10% higher than those presented in Ref. 12.

[12] W. B. Richards, C. B. Chiu, R. D. Eandi, A. C. Helmholz, R. W. Kenney, B. J. Moyer, J. A. Poirier, R. J. Cence, V. Z. Peterson, N. K. Sehgal, and V. J. Stenger, Phys. Rev. Letters **16**, 1221 (1966); C. B. Chiu, R. D. Eandi, A. C. Helmholz, R. W. Kenney, B. J. Moyer, J. A. Poirier, W. B. Richards, R. J. Cence, V. Z. Peterson, N. K. Sehgal, and V. J. Stenger, Phys. Rev. **156**, 1415 (1967).

ACKNOWLEDGMENTS

We would like to thank B. Dainese, Thomas Lyons, and their respective groups for their tireless assistance in the development, construction, and operation of the spark-chamber system, and to express our gratitude to Dr. B. Gottschalk for providing much of the fast electronic circuitry. We also acknowledge the contributions of Dr. R. Panvini in the early stages of this work. We are indebted to the entire staff of the Brookhaven National Laboratory Cosmotron and to our respective scanning groups, without whose expert assistance and support the experiment could not have been performed.

APPENDIX A: BEAM MOMENTUM DETERMINATION

Eleven nominal values of central momenta were selected for the incident π^-'s. The magnet currents and fields were set at the design values and the magnetic fields of the momentum-resolving magnets were measured by NMR and continuously monitored by Hall-effect probes previously calibrated against the NMR. The kinematics of two of the reactions being studied in this experiment ($\pi^- p \rightarrow \pi^0 n$, $\pi^- p \rightarrow \eta^0 n$) provide the best check available to us upon the momentum.

We have made use of the characteristic opening-angle distributions and minima of both the π^0 and η^0 to measure the incident momenta. The sensitivity of this technique can be seen from Fig. 13, where $d\Theta/dp$ are plotted for the pion and η-meson minimum opening angles as a function of momentum. The theoretically expected distributions for the two-γ-ray opening angles

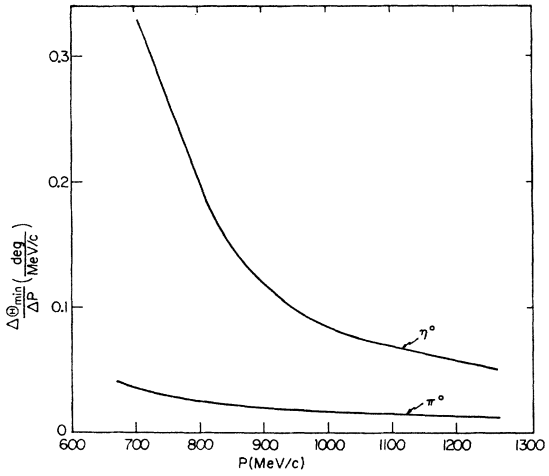

FIG. 13. Sensitivity $(\Delta\Theta/\Delta p)_{\text{min}}$ of the minimum-opening-angle determination of the incident π momentum as a function of the momentum for the π^0 and η^0.

TABLE VIII. Beam-momentum determination from opening-angle distribution.

Beam momentum (MeV/c)	$(\Delta\Theta_{\min}/\Delta p)/\pi$ °/(MeV/c)	$(\Delta\Theta_{\min}/\Delta p)/\eta^0$ °/(MeV/c)
654	0.040	...
694	0.033	0.33
729	0.033	0.29
755	0.029	0.25
811	0.025	0.17
862	0.022	0.14
928	0.019	0.10
978	0.017	0.08
1024	0.016	0.08
1099	0.014	0.07
1247	0.013	0.05

from π^0 and η^0 at any given momentum are calculated by the Monte Carlo technique using the appropriate angular distribution, low-energy γ-ray cutoff for detection, measuring resolution, and normalizing to the same number of events in an opening-angle interval. These expected distributions are then separately compared to the experimental opening-angle distributions. If comparison shows that a theoretical and experimental distribution do not agree, then a new theoretical distribution is calculated at a slightly different incident momentum and comparison made again. The process is repeated until agreement is reached. In practice this procedure usually takes one iteration. The errors on the momenta as determined by the opening angles correspond to a shift in the position of $\Theta_{\min}$ by $\pm 0.25°$. Over-all shifts of 0.5° are readily detectable and therefore it is felt that this error is adequate. The effect of other parameters affecting this momentum determination, including the low-energy γ-ray cutoff for detection, the target position, the beam-momentum spread, and the background subtraction, were all investigated and found to give consistent momentum values within their error limits. A summary of these results is given in Table VIII.

APPENDIX B: CORRECTION FACTORS FOR σ_N CALCULATION

The fraction F_2, appearing in Eq. (5), results from events which have charged particles associated with them, but appear as neutral events because all of the charged particles escape detection. We have calculated F_2 using Monte Carlo techniques and available data[13] on branching ratios to charged final states and angular distributions. Because of our tight electronic geometry and the high multiplicity of prongs in inelastic events, F_2 is found to be negligible. We take it equal to zero.

The remaining fraction $1-F_1$ corrects for the loss of true neutral events which are rejected by the electronic logic because of the presence of a spurious particle. These spurious particles arise from two types of events. The first are events which have a sufficiently energetic and appropriately directed δ ray (produced either in the array of thin foils, counters, or liquid hydrogen through which the beam passes) which reaches the anticoincidence counter removing the event from the count. The second are events associated with a neutron or γ ray which interacts in the target walls or anticoincidence counter, giving a charged prong which removes the event from the count.

We use the total number of parent events in the various reaction channels involved in producing our observed events, as indicated in Sec. IV, to evaluate the correction $1-F_1$. To this end, we form the ratio

$$f=\sum_i S_i/\sum_j P_j, \tag{B1}$$

where S_i is the number of events of topology i found in scanning and P_j is the number of parents deduced in channel j; the summations are extended over all possible configurations. This fraction f has in it the effect of the neutron and γ-ray conversion in the anticoincidence shield via the elements P_{jk}.

A second fraction f' is calculated from geometry and known electromagnetic cross sections to give the fraction of all events which do not have a δ ray associated with them capable of giving anticoincidence. This fraction has a value of 0.998 typically. Thus $ff'=1-F_1$.

APPENDIX C: CHOICE OF EFFECTIVE LOW-ENERGY CUTOFF

The number of sparks appearing in any given shower depends upon plate thickness, the energy of the electrons which propagate through the plates, the angle the shower makes with the normal to the plates, and the efficiency of the gaps for detecting them. Thus a fixed number (three in our case) of sparks defining a minimum for acceptance as a γ ray corresponds to different effective minimum-energy γ rays at each set of running conditions. All of these effects may be accounted for to obtain an internally consistent sample by finding experimentally a value for what we call the effective low-energy cutoff. It is found that a value in the range 40 ± 10 MeV is adequate for all the data.

In order to find this value, several tests are made on the data at each incident momentum. Consequently, eleven separate evaluations are made. The tests are as

TABLE IX. Effective low-energy cutoff.

Momentum (MeV/c)	Low-energy cutoff (MeV)	Momentum (MeV/c)	Low-energy cutoff (MeV)
654	50	862	40
694	30	928	35
729	40	978	35
755	45	1024	30
811	35	1099	45
		1247	35

[13] M. B. Olsson and G. B. Yodh, Phys. Rev. **145**, 1309 (1966).

follows:

(1) χ^2 fit for the number of parents is made to the observed numbers of γ-ray multiplicities including all multiplicities 0–6. This fit is made as a function of the cutoff since the Monte Carlo-calculated P_{jk}'s depend slightly on it.

(2) A comparison is made of the number of π^0 parents predicted from multiplicites to that number predicted by the angular-distribution method (see Secs. IV and V). This is made as a function of the cutoff, varying it in steps of 5 MeV between 30 and 60 MeV for all tests.

(3) Same tests as (2) except for parent numbers of η^0.

(4) The observed number of two-γ-ray events falling in the opening-angle region between the π^0 peak and the η^0 peak is compared with the number of two-γ-ray events to be subtracted as background, predicted by the parent fit in all channels. This comparison is made as a function of the cutoff.

Test (1) shows a broad minimum in the value of χ^2 as a function of the cutoff, while the other three tests show minima in the normalized difference between the two compared quantities. The value of the cutoff chosen for a given sample is that value which gives best coincidence of maxma and minima for all four tests. The values found in the different samples range from 30 to 50 MeV; thus they are consistent with an over-all choice of 40 ± 10 MeV. The specific values chosen for the data taken at each of the running conditions are shown in Table IX.

APPENDIX D: COMPLETE ERROR MATRICES FOR π^0 AND η^0 ANGULAR DISTRIBUTIONS

Tables X and XI give the complete error matrices[14] for the Legendre-polynomial expansions of the π^0 and η^0

TABLE X. Legendre-polynomial coefficient error matrices for π^0. Units are $(\text{mb/sr})^2$ with the same normalization as in text. Here $N(n)$ means $N\times10^n$.

(a) 654 MeV/c

0.70620(−4)	0.79069(−4)	0.50750(−4)	−0.64275(−5)	0.27197(−4)	0.50040(−4)	0.30229(−4)
0.79069(−4)	0.27615(−3)	0.15135(−3)	0.12929(−3)	0.50991(−4)	0.75735(−4)	0.62907(−4)
0.50736(−4)	0.15135(−3)	0.48321(−3)	0.30613(−3)	0.21002(−3)	0.53241(−5)	0.24405(−4)
−0.64283(−5)	0.12929(−3)	0.30613(−3)	0.72418(−3)	0.36811(−3)	0.21730(−3)	−0.20560(−4)
0.27210(−4)	0.50991(−4)	0.21002(−3)	0.36811(−3)	0.93267(−3)	0.46776(−3)	0.27576(−3)
0.50040(−4)	0.75735(−4)	0.53241(−5)	0.21730(−3)	0.46776(−3)	0.11846(−2)	0.56596(−3)
0.30229(−4)	0.62907(−4)	0.24405(−4)	−0.20560(−4)	0.27576(−3)	0.56596(−3)	0.14245(−2)

(b) 694 MeV/c

0.49548(−4)	0.53419(−4)	0.43695(−4)	−0.41692(−5)	0.88542(−5)	0.35663(−4)	0.32607(−5)
0.53418(−4)	0.20460(−3)	0.10363(−3)	0.93429(−4)	0.41334(−4)	0.24979(−4)	0.72667(−4)
0.43701(−4)	0.10364(−3)	0.33319(−3)	0.21968(−3)	0.13888(−3)	0.15770(−4)	−0.28644(−4)
−0.41692(−5)	0.93429(−4)	0.21969(−3)	0.48668(−3)	0.28517(−3)	0.17209(−3)	0.18890(−4)
0.88542(−5)	0.41340(−4)	0.13888(−3)	0.28517(−3)	0.64015(−3)	0.35610(−3)	0.22489(−3)
0.35663(−4)	0.24979(−4)	0.15770(−4)	0.17209(−3)	0.35610(−3)	0.78427(−3)	0.35911(−3)
0.32607(−5)	0.72667(−4)	−0.28644(−4)	0.18890(−4)	0.22489(−3)	0.35911(−3)	0.89206(−3)

(c) 729 MeV/c

0.56500(−4)	0.38101(−4)	0.45753(−4)	−0.25068(−5)	0.31952(−5)	0.51782(−4)	−0.13107(−4)
0.38101(−4)	0.22652(−3)	0.77239(−4)	0.88777(−4)	0.64813(−4)	−0.51389(−5)	0.97515(−4)
0.45753(−4)	0.77246(−4)	0.35650(−3)	0.19976(−3)	0.10162(−3)	0.32871(−4)	−0.52413(−4)
−0.25068(−5)	0.88785(−4)	0.19976(−3)	0.49223(−3)	0.24435(−3)	0.15249(−3)	0.44923(−4)
0.31881(−5)	0.64813(−4)	0.10162(−3)	0.24435(−3)	0.67668(−3)	0.29833(−3)	0.21846(−3)
0.51782(−4)	−0.51389(−5)	0.32871(−4)	0.15249(−3)	0.29833(−3)	0.89839(−3)	0.34755(−3)
−0.13107(−4)	0.97515(−4)	−0.52413(−4)	0.44923(−4)	0.21846(−3)	0.34755(−3)	0.10254(−2)

(d) 755 MeV/c

0.51738(−4)	0.13728(−4)	0.34317(−4)	0.13203(−5)	−0.61383(−5)	0.56655(−4)	−0.25610(−4)
0.13728(−4)	0.19625(−3)	0.35603(−4)	0.53597(−4)	0.78210(−4)	−0.38969(−4)	0.93833(−4)
0.34317(−4)	0.35603(−4)	0.29532(−3)	0.13727(−3)	0.37249(−4)	0.48378(−4)	−0.60906(−4)
0.13199(−5)	0.53603(−4)	0.13727(−3)	0.39842(−3)	0.14372(−3)	0.88268(−4)	0.79968(−4)
−0.61446(−5)	0.78210(−4)	0.37249(−4)	0.14372(−3)	0.57277(−3)	0.17881(−3)	0.14359(−3)
0.56655(−4)	−0.38969(−4)	0.48378(−4)	0.88268(−4)	0.17881(−3)	0.78139(−3)	0.18393(−3)
−0.25610(−4)	0.93833(−4)	−0.60906(−4)	0.79968(−4)	0.14359(−3)	0.18393(−3)	0.97601(−3)

(e) 811 MeV/c

0.12381(−3)	−0.69231(−4)	0.10735(−3)	0.23941(−4)	−0.64922(−4)	0.18295(−3)	−0.11803(−3)
−0.69233(−4)	0.50404(−3)	−0.91528(−4)	0.10755(−3)	0.30622(−3)	−0.24427(−3)	0.37516(−3)
0.10737(−3)	−0.91528(−4)	0.66346(−3)	0.13521(−3)	−0.15505(−4)	0.35950(−3)	−0.25236(−3)
0.23941(−4)	0.10755(−3)	0.13521(−3)	0.83348(−3)	0.13468(−3)	0.96267(−4)	0.30450(−3)
−0.64922(−4)	0.30622(−3)	−0.15505(−4)	0.13468(−3)	0.12293(−2)	−0.64460(−4)	0.26526(−3)
0.18295(−3)	−0.24427(−3)	0.35950(−3)	0.96267(−4)	−0.64460(−4)	0.17508(−2)	−0.22395(−3)
−0.11803(−3)	0.37516(−3)	−0.25236(−3)	0.30450(−3)	0.26526(−3)	−0.22395(−3)	0.23453(−2)

[14] For a discussion of the error matrix, see, e.g., N. Arley and K. R. Buch, *Introduction to the Theory of Probability and Statistics* (John Wiley & Sons, Inc., New York, 1950), Chap. 12.

TABLE X. (*continued*)

(f) 862 MeV/c

0.46590(−4)	−0.47545(−4)	0.50472(−4)	0.21501(−4)	−0.35423(−4)	0.83484(−4)	−0.43752(−4)
−0.47545(−4)	0.19782(−3)	−0.55139(−4)	0.40676(−4)	0.16620(−3)	−0.10906(−3)	0.13770(−3)
0.50476(−4)	−0.55142(−4)	0.22194(−3)	0.45216(−4)	−0.25273(−4)	0.16504(−3)	−0.82097(−4)
0.21501(−4)	0.40680(−4)	0.45216(−4)	0.26952(−3)	0.23043(−4)	0.44179(−4)	0.16440(−3)
−0.35423(−4)	0.16620(−3)	−0.25273(−4)	0.23043(−4)	0.38559(−3)	−0.57054(−4)	0.11583(−3)
0.83484(−4)	−0.10906(−3)	0.16504(−3)	0.44179(−4)	−0.57054(−4)	0.51990(−3)	−0.93721(−4)
−0.43752(−4)	0.13770(−3)	−0.82097(−4)	0.16440(−3)	0.11583(−3)	−0.93721(−4)	0.62824(−3)

(g) 928 MeV/c

0.91835(−4)	−0.94013(−4)	0.11485(−3)	0.40983(−4)	−0.58646(−4)	0.18448(−3)	−0.10383(−3)
−0.94013(−4)	0.40466(−3)	−0.98935(−4)	0.13067(−3)	0.36200(−3)	−0.20457(−3)	0.30767(−3)
0.11486(−3)	−0.98939(−4)	0.44911(−3)	0.12142(−3)	−0.25410(−4)	0.33461(−3)	−0.11827(−3)
0.40984(−4)	0.13068(−3)	0.12141(−3)	0.51933(−3)	0.76368(−4)	0.14357(−3)	0.32053(−3)
−0.58646(−4)	0.36200(−3)	−0.25410(−4)	0.76368(−4)	0.76961(−3)	−0.12369(−3)	0.32622(−3)
0.18448(−3)	−0.20457(−3)	0.33461(−3)	0.14357(−3)	−0.12369(−3)	0.10120(−2)	−0.18294(−3)
−0.10383(−3)	0.30767(−3)	−0.11827(−3)	0.32053(−3)	0.32622(−3)	−0.18294(−3)	0.11682(−2)

(h) 978 MeV/c

0.14096(−3)	−0.11982(−3)	0.18084(−3)	0.57834(−4)	−0.60275(−4)	0.29446(−3)	−0.15214(−3)
−0.11982(−3)	0.62728(−3)	−0.10839(−3)	0.25720(−3)	0.55034(−3)	−0.24924(−3)	0.51273(−3)
0.18082(−3)	−0.10839(−3)	0.72727(−3)	0.23963(−3)	0.42694(−4)	0.49314(−3)	−0.17381(−3)
0.57836(−4)	0.25721(−3)	0.23964(−3)	0.85331(−3)	0.19443(−3)	0.25147(−3)	0.47319(−3)
−0.60275(−4)	0.55034(−3)	0.42694(−4)	0.19443(−3)	0.12199(−2)	−0.96163(−4)	0.55866(−3)
0.29446(−3)	−0.24924(−3)	0.49314(−3)	0.25147(−3)	−0.96163(−4)	0.16213(−2)	−0.22932(−3)
−0.15214(−3)	0.51273(−3)	−0.17381(−3)	0.47319(−3)	0.55866(−3)	−0.22932(−3)	0.18963(−2)

(i) 1024 MeV/c

0.10927(−3)	−0.94662(−4)	0.12836(−3)	0.20055(−4)	−0.34789(−4)	0.21837(−3)	−0.12383(−3)
−0.94663(−4)	0.47346(−3)	−0.11768(−3)	0.19880(−3)	0.35735(−3)	−0.18062(−3)	0.37564(−3)
0.12837(−3)	−0.11768(−3)	0.57403(−3)	0.11745(−3)	0.62757(−4)	0.29702(−3)	−0.74965(−4)
0.20055(−4)	0.19880(−3)	0.11745(−3)	0.68327(−3)	0.61142(−4)	0.23575(−3)	0.29199(−3)
−0.34799(−4)	0.35735(−3)	0.62757(−4)	0.61142(−4)	0.10383(−2)	−0.13140(−3)	0.46752(−3)
0.21837(−3)	−0.18062(−3)	0.29702(−3)	0.23575(−3)	−0.13140(−3)	0.13501(−2)	−0.25921(−3)
−0.12383(−3)	0.37564(−3)	−0.74965(−4)	0.29199(−3)	0.46752(−3)	−0.25921(−3)	0.15320(−2)

(j) 1099 MeV/c

0.52513(−4)	−0.35827(−4)	0.33488(−4)	−0.36087(−5)	−0.58172(−5)	−0.97476(−4)	−0.31208(−4)	−0.35139(−5)	0.28337(−5)
−0.35834(−4)	0.19969(−3)	−0.77507(−4)	0.54260(−4)	0.12186(−3)	−0.52051(−4)	0.15950(−3)	−0.50132(−4)	−0.12193(−4)
0.33488(−4)	−0.77507(−4)	0.31017(−3)	0.29252(−4)	0.40417(−4)	0.11178(−3)	−0.40648(−4)	0.21442(−3)	−0.38844(−4)
−0.36159(−5)	0.54253(−4)	0.29259(−4)	0.39805(−3)	−0.27585(−4)	0.94720(−4)	0.12304(−3)	−0.28220(−5)	0.25855(−3)
−0.57955(−5)	0.12186(−3)	0.40417(−4)	−0.27585(−4)	0.51053(−3)	−0.92663(−4)	0.12345(−3)	0.87112(−4)	0.14319(−4)
0.97469(−4)	−0.52051(−4)	0.11178(−3)	0.94720(−4)	−0.92671(−4)	0.69438(−3)	−0.13929(−3)	0.12574(−3)	0.10211(−3)
−0.31208(−4)	0.15950(−3)	−0.40764(−4)	0.12304(−3)	0.12356(−3)	−0.13929(−3)	0.85831(−3)	−0.21825(−3)	0.23249(−3)
−0.35139(−5)	−0.50132(−4)	0.21442(−3)	−0.28220(−5)	0.87112(−4)	0.12574(−3)	−0.21825(−3)	0.10934(−2)	−0.15861(−3)
0.28337(−5)	−0.12193(−4)	−0.38844(−4)	0.25855(−3)	0.14319(−4)	0.10211(−3)	0.23249(−3)	−0.15861(−3)	0.12812(−2)

(k) 1247 MeV/c

0.25339(−4)	−0.15329(−4)	0.15862(−4)	−0.10305(−4)	0.22660(−5)	0.19961(−4)	−0.91757(−5)	−0.48722(−5)	−0.11595(−4)
−0.15325(−4)	0.95696(−4)	−0.45502(−4)	0.32055(−4)	0.10044(−4)	−0.75694(−5)	0.27982(−4)	−0.30974(−4)	−0.57418(−6)
0.15802(−4)	−0.45547(−4)	0.15880(−3)	−0.35775(−4)	0.34407(−4)	−0.50984(−5)	−0.27549(−4)	0.57919(−4)	−0.44224(−4)
−0.10301(−4)	0.32014(−4)	−0.35827(−4)	0.20936(−3)	−0.65262(−4)	0.31459(−4)	0.54823(−5)	−0.18769(−4)	0.50834(−4)
0.22660(−5)	0.10044(−4)	0.34407(−4)	−0.65262(−4)	0.26220(−3)	−0.76357(−4)	0.51879(−4)	−0.12851(−4)	−0.24806(−4)
0.19961(−4)	−0.75694(−5)	−0.50984(−5)	0.31459(−4)	−0.76357(−4)	0.35422(−3)	−0.10655(−3)	0.49170(−4)	0.24835(−5)
−0.91757(−5)	0.27985(−4)	−0.27609(−4)	0.54823(−5)	0.51879(−4)	−0.10655(−3)	0.43837(−3)	−0.12158(−3)	0.10983(−3)
−0.48722(−5)	−0.30974(−4)	0.57919(−4)	−0.18769(−4)	−0.12851(−4)	0.49170(−4)	−0.12158(−3)	0.58772(−3)	−0.16575(−3)
−0.11595(−4)	−0.57418(−6)	−0.44224(−4)	0.50834(−4)	−0.24806(−4)	0.24835(−5)	0.10983(−3)	−0.16575(−3)	0.68156(−3)

TABLE XI. Legendre-polynomial coefficient error matrices for η^0. Units are (mb/sr)^2 with the same normalization as in text.

(a) 755 MeV/c

0.11226(−4)	0.25340(−5)	0.13372(−5)
0.25340(−5)	0.44034(−4)	0.55258(−5)
0.13372(−5)	0.55258(−5)	0.97386(−4)

(b) 811 MeV/c

0.33317(−4)	−0.52786(−5)	0.57899(−5)
−0.52786(−5)	0.13046(−3)	0.48430(−5)
0.57899(−5)	0.48430(−5)	0.28882(−3)

TABLE XI. (*continued*)

		(c) 862 MeV/c		
0.11184(−4)	−0.42353(−6)	0.34315(−5)	−0.31309(−5)	−0.38237(−5)
−0.42355(−6)	0.43599(−4)	−0.67696(−5)	0.17928(−5)	−0.59815(−5)
0.34315(−5)	−0.67696(−5)	0.90881(−4)	−0.12056(−4)	−0.12102(−4)
−0.31309(−5)	0.17928(−5)	−0.12056(−4)	0.18145(−3)	−0.34556(−4)
−0.38237(−5)	−0.59815(−5)	−0.12102(−4)	−0.34556(−4)	0.39330(−3)
		(d) 928 MeV/c		
0.12000(−4)	−0.23130(−5)	0.18398(−5)	−0.34887(−5)	−0.44264(−5)
−0.23130(−5)	0.43844(−4)	−0.11608(−4)	−0.67118(−6)	−0.78592(−5)
0.18402(−5)	−0.11608(−4)	0.89343(−4)	−0.21225(−4)	−0.82633(−5)
−0.34887(−5)	−0.67118(−6)	−0.21225(−4)	0.17468(−3)	−0.26383(−4)
−0.44264(−5)	−0.78592(−5)	−0.82633(−5)	−0.26383(−4)	0.40586(−3)
		(e) 978 MeV/c		
0.37482(−4)	0.66747(−5)	0.41473(−5)	−0.14733(−4)	−0.30108(−4)
0.66746(−5)	0.13901(−3)	−0.15319(−4)	−0.36005(−4)	0.10381(−4)
0.41489(−5)	−0.15319(−4)	0.26846(−3)	0.13295(−4)	−0.64073(−4)
−0.14733(−4)	−0.36005(−4)	0.13295(−4)	0.60871(−3)	−0.10474(−3)
−0.30108(−4)	0.10381(−4)	−0.64073(−4)	−0.10474(−3)	0.15537(−2)
		(f) 1024 MeV/c		
0.17334(−4)	−0.26913(−5)	−0.31229(−5)	0.25961(−6)	−0.43189(−5)
−0.26913(−5)	0.56073(−4)	−0.11996(−4)	−0.53376(−5)	−0.23376(−5)
−0.31223(−5)	−0.11996(−4)	0.12554(−3)	−0.37568(−4)	−0.19215(−4)
0.25961(−6)	−0.53376(−5)	−0.37568(−4)	0.22863(−3)	−0.16739(−4)
−0.43189(−5)	−0.23376(−5)	−0.19215(−4)	−0.16739(−4)	0.42122(−3)
		(g) 1099 MeV/c		
0.15539(−4)	0.37552(−5)	−0.53048(−5)	0.28937(−5)	−0.19431(−4)
0.37552(−5)	0.47434(−4)	−0.22113(−5)	−0.13203(−4)	−0.44143(−5)
−0.53048(−5)	−0.22113(−5)	0.10396(−3)	−0.48321(−4)	0.58140(−4)
0.28937(−5)	−0.13203(−4)	−0.48321(−4)	0.32199(−3)	−0.23671(−3)
−0.19431(−4)	−0.44143(−5)	0.58140(−4)	−0.23671(−3)	0.64484(−3)
		(h) 1247 MeV/c		
0.10268(−4)	0.28939(−5)	−0.36167(−5)	−0.36375(−5)	−0.45576(−5)
0.28939(−5)	0.30748(−4)	−0.14002(−5)	−0.13972(−4)	0.17405(−5)
−0.36165(−5)	−0.14002(−5)	0.63016(−4)	0.34857(−5)	−0.33906(−4)
−0.36375(−5)	−0.13972(−4)	0.34857(−5)	0.10541(−3)	0.49102(−5)
−0.45576(−5)	0.17405(−5)	−0.33906(−4)	0.49102(−5)	0.22176(−3)

angular distributions. A word of caution is in order. These matrices contain the statistical error associated with the fit only; they do not include the errors associated with the determination of the π^0 and η^0 cross sections (and quoted in Table V) which systematically shift all coefficients in a distribution. The two errors are illustrated graphically in Figs. 6 and 7, where the error bars for the 0° and 180° cross sections have had them compounded, while the error bar shown at an intermediate value of $\cos\theta$ is that of the fit only.

APPENDIX E: GEOMETRIC DEPENDENCE OF FITTED ANGULAR DISTRIBUTIONS

The suggestion has been made[12] that in a γ-ray detection geometry such as is used in this experiment, the difference between a uniform angular distribution and one which is of the form $1+\cos^2$ cannot be distinguished with certainty. This suggestion is certainly correct in the sense that no measurement of finite statistics ever represents "certainty"; however, as it bears upon this experiment, it has relevance only to statistics and not to geometry. This can easily be shown by standard statistical tests on our data. At most momenta the number of η^0 parents is of the order of 1000. At 811 MeV/c they are about 400. As discussed in Sec. V, Legendre-polynomial fits are made to the resulting angular distributions and errors are generated as described. The errors on these coefficients should reflect in the accepted statistical sense the probability that the observed distribution differs from the true one. More specifically, they should give a quantitative measure of the probability that both C_1 and C_2 might be simultaneously zero when the true distribution had

nonzero C_1 and C_2. We have checked the validity of the assigned errors by making Monte Carlo simulations of a number of statistical samples of 400 and 1000 events. In both cases, the angular distribution used in the Monte Carlo simulation was that of Ref. 12 for 704-MeV incident π^- kinetic energy. It was found that the values of the coefficients resulting from fits to distributions were normally distributed with half-widths equal to the calculated errors. The chance that in a population of 400 parents the given distribution would be mistakenly called isotropic was 1 in 23; for the 1000-event population the chance was 1 in 2000. Thus we conclude that our errors as presented in this paper correctly represent the experimental situation.

PHYSICAL REVIEW VOLUME 187, NUMBER 5 25 NOVEMBER 1969

Spin Analysis of $p\pi^+\pi^-$ Enhancements in the $pp\pi^+\pi^-$ Final State Produced in pp Interactions at 22 GeV/c*

J. I. RHODE, R. A. LEACOCK, W. J. KERNAN, R. A. JESPERSEN, AND T. L. SCHALK
Institute for Atomic Research and Department of Physics, Iowa State University, Ames, Iowa 50010
(Received 28 July 1969)

We have investigated decay angular distributions and other characteristics associated with enhancements near 1450 and 1700 MeV in the $p\pi^+\pi^-$ mass distribution for the $pp\pi^+\pi^-$ final state produced in pp interactions at 22 GeV/c. Our results are consistent with a spin assignment of $\frac{1}{2}$ for the 1450-MeV effect if the $\Delta^{++}\pi^-$ branching of this effect is assumed to be small. We associate this effect with the $P_{11}(1470)$ state inferred from phase-shift analyses. In the case of the 1700-MeV feature, we favor strong contributions from a $J=\frac{5}{2}^+$ state which can be reasonably associated with the $F_{15}(1690)$ state reported in the phase-shift work.

I. INTRODUCTION

IN an analysis of two- and four-prong events from a 75 000-frame exposure of the Brookhaven National Laboratory 80-in. hydrogen bubble chamber to 22-GeV/c protons, we have investigated the following reactions:

$$pp \to pn\pi^+, \quad 220 \text{ events} \quad (1)$$

$$\to pp\pi^+\pi^-, \quad 1234 \text{ events}. \quad (2)$$

Preliminary studies of certain aspects of these final states have been reported previously.[1,2]

We consider here characteristics of two significant enhancements in the $p\pi^+\pi^-$ (and $\Delta^{++}\pi^-$) mass distributions [Fig. 1(a)] for reaction (2), one with mass 1443±15 MeV, width 100±15 MeV, and the second of mass 1693±15 MeV, width 235±50 MeV.[3] We refer to these features as the 1450- and 1700-MeV effects, respectively. Evidence for a two-peak structure in the $p\pi^+\pi^-$ mass spectrum for this and other reactions at various momenta have been noted by other workers.[4–6]

Reaction (2) is characterized by a very strong forward and backward peaking of the final-state baryons in the

* Work performed in part in the Ames Laboratory of the U. S. Atomic Energy Commission. Contribution No. 2598.

[1] R. A. Jespersen, Y. W. Kang, W. J. Kernan, R. A. Leacock, J. I. Rhode, T. L. Schalk, and L. S. Schroeder, Phys. Rev. Letters **21**, 1368 (1968).

[2] R. A. Jespersen, Y. W. Kang, W. J. Kernan, R. A. Leacock, J. I. Rhode, T. L. Schalk, and L. S. Schroeder, in Third Topical Conference on Resonant Particles, Ohio University, Athens, Ohio, 1967 (unpublished).

[3] In quoting masses and widths for these effects we are simply parametrizing features of our data. We can not demonstrate from the $p\pi^+\pi^-$ mass spectrum alone that either of these effects (but especially the 1700-MeV peak) can be associated with a single resonance. In Ref. 1 it was shown that the $p\pi^+\pi^-$ mass distribution for reaction (1) is poorly represented by either a conventional "Deck" background (with or without reasonable refinements in form factors) or by this background plus a single broad resonance. The data are, however, adequately accounted for by two resonance structures plus the Deck background. E. L. Berger *et al.* [Phys. Rev. Letters **20**, 964 (1968)] have shown that a Reggeized Deck calculation is in better agreement with certain features of reaction (1) (at lower momenta) than the original Deck model. Such modifications of the Deck effect are, however, generally unable to account for the sharpness of the 1450-MeV effect seen in our and in certain other workers' data (especially at high energies), and, in any case, cannot reproduce a double-peak structure (see Ref. 6). Nevertheless, these calculations may still be valid, according to the duality concept [R. Dolen, D. Horn, and C. Schmid, Phys. Rev. **166**, 1768 (1968); G. F. Chew and A. Pignotti, Phys. Rev. Letters **20**, 1078 (1968)], in the sense of giving correctly a local average over direct-channel resonance effects. In this view, resonance states in our $\Delta^{++}\pi^-$ channel are already accounted for by (and are not superposed upon) the π trajectory exchange in the crossed channel. If this is correct, then fits to the $p\pi^+\pi^-$ and $\Delta^{++}\pi^-$ mass distributions using resonances plus Deck background will lead to an underestimate of the resonance contribution. Our analysis here is not dependent upon the validity of this approach, although certain arguments in the text, particularly that concerning the $\Delta^{++}\pi^-$ branching of the 1700-MeV effect, are strengthened if this viewpoint is adopted.

[4] S. P. Almeida, J. G. Rushbrooke, J. H. Scharenguivel, M. Behrens, V. Blobel, I. Borecka, H. C. Dehne, J. Diaz, G. Knies, A. Schmitt, K. Strömer, and W. P. Swanson, Phys. Rev. **174**, 1638 (1968).

[5] R. Ehrlich, R. Nieporent, R. J. Plano, J. B. Whittaker, C. Baltay, J. Feinman, P. Franzini, R. Newman, and N. Yeh, Phys. Rev. Letters **21**, 1839 (1968).

[6] J. G. Rushbrooke, in *Proceedings of the Fourteenth International Conference on High-Energy Physics, Vienna, 1968*, edited by J. Prentki and J. Steinberger (CERN, Geneva, 1968), p. 159.